Ionization of Solute Molecules at the Liquid Water Surface, Interfaces, and Self-Assembled Systems

Harata, Akira
Kyushu University

Sato, Miki
Kyushu University

Ishioka, Toshio
Kyushu University

出版情報：pp.445-, 2010-12-13. CRC Press Inc
バージョン：
権利関係：This is an Accepted Manuscript of a book chapter published by Routledge/CRC Press in [Charged Particle and Photon Interactions with Matter : Recent Advances, Applications, and Interfaces] on 2010, available online: http://www.routledge.com/9781439811771 or http://www.crcpress.com/9781439811771

Ionization of solute molecules at the liquid water surface, interfaces, and self-assembled systems

Akira Harata*, Miki Sato, and Toshio Ishioka

Faculty of Engineering Sciences, Kyushu University
Kasugakoen 6-1, Kasuga-shi, Fukuoka 816-8580, Japan

*Tel: +81-92-583-7552 ; fax: +81-92-583-7557
Email address: harata@mm.kyushu-u.ac.jp (A. Harata)

Keywords: Interface-selective spectroscopy, Liquid water surface, Aqueous solution, Solute molecules, Self-assembled layer, Synchrotron photoionization, Laser multi-photon ionization, Laser second harmonic generation, Surface tension, Photoionization spectra, Photoionization threshold, Molecular orientation, Adsorption equilibrium, Detection limit, Acid-base equilibrium, Monitoring of volatile molecules

Abstract

Studies on the photoionization measurements of solute molecules adsorbed at the liquid water surface are summarized for the molecular -level understanding at the surface. Interface selective observation methods are overlooked with a view point of detection sensitivity. It is pointed out that a photoionization measurement with moderate sensitivity, fine surface selectivity, and good applicability is an attractive technique for observing solute molecules at the water surface. The methods for measurements of photoionization current spectra, laser multi-photon ionization current, laser second harmonic generation and surface tension are described. Some discussion on photoionization thresholds, polarization- and concentration dependence, and surface molecular monitoring are presented of surface-adsorbed molecules, based on experimental data.

Table of Contents

1. General comments

1.1. Introduction

Liquid interfaces are of fundamental and practical importance in science and technology (Birdi, 1997; 1999; Jungwirth et al., 2006a). Understanding the molecular behavior at the interface involves fundamental sciences of molecular interaction and assists with the resolution of a variety of problems related to chemistry, physics, life and environmental sciences. Among liquid interfaces, the air-water interface (water surface) is the most universal and may be the most important.

Many studies have targeted the molecular behavior at liquid interfaces experimentally (Shen et al., 2006; Gopalakrishnan et al., 2006; Winter and Faubel, 2006; Benjamin, 2006; Davidovits et al., 2006; Donaldson and Vaida 2006) and theoretically (Benjamin, 2006; Perry et al. 2006; Jungwirth and Tobias, 2006b; Mundy and Kuo, 2006; Chang and Dang, 2006; Garret et at al., 2006). These studies have clarified that molecules at a solution interface behave differently from those of the same chemical species in a bulk solution. It is natural to consider that, primarily, the inhomogeneous and thermally fluctuating structure in the vicinity of the top surface of the half-space filled with solvent molecules dominates the interfacial properties of solute molecules adsorbed. Additionally, solute-solute interaction in the interface region influences the molecular behavior.

Fundamental interests in solute molecules at the liquid water surface include depth distribution, orientation, molecular interaction, adsorption-desorption dynamics, surface diffusion, and influence of the bulk properties of solvent liquid on these from both the static (time-averaged) and dynamic points of view. For applications to chemical processing and material fabrication using a liquid surface, such as the Langmuir-Blodgett technique, precise control of the molecular behavior at the interface might provide a novel way to control the properties of the materials produced.

To precisely understand and control the molecular behavior at the interface, methodologies for observing molecules at the interface play important roles. Interface-selective observation methods are required because it is typical for a large amount of the same species of the target solute molecules to be in a bulk solution. Furthermore, a highly sensitive performance is preferable for this method because the absolute amount of the interface-adsorbed species is smaller than 1 nano-mole/cm^2.

1.2. Thermodynamic view of the water surface

The water surface is thermally fluctuating. Thermodynamic theory predicts a time-averaged view of the liquid surface (Benjamin, 1996; 2006). As shown in Fig. 1, the water surface has a transition region of mass density with a finite thickness. The density distribution along the surface normal is described as a coerror function with a parameter representing the half-width of the transition

region: the thickness of the water surface can be defined as 2σ, which is given as

$$2\sigma = \sqrt{\frac{kT}{\pi\gamma}\ln\frac{1+(2\pi l_c/\xi)^2}{1+(2\pi l_c)^2/S}}, \quad (1)$$

where γ is the surface tension, S is the surface area of liquid, k is the Boltzmann constant, T is the temperature, ξ is the bulk correlation length (0.6 - 0.9 nm). Here l_c is the capillary length equal to $(\gamma/\rho_0 g)^{1/2}$,with ρ_0 the mass density, and g the acceleration due to gravity.

The thickness of the pure water surface is estimated to be 0.8 nm at 300K, which is comparable to the size of an organic molecule. Surface tension has a strong influence on the thickness. Smaller surface tension, typically induced by the addition of organic molecules in the water, makes the transition region thinner. It is notable that these molecules are dynamically moving in, adsorbing to, and desorbing from the transition region.

Traditionally, surface tension measurements have been made to thermodynamically understand a state of solute molecules adsorbed at the water surface. Surface excess Γ is a function of the surface tension and the solute concentration C in a bulk solution as (Motomura, 1978; Motomura at al., 1981),

$$\Gamma = -\frac{C}{vRT}\left(\frac{\partial\gamma}{\partial C}\right)_{T,P}, \quad (2)$$

where R is the universal gas constant, P is the pressure, and v represents the number of ions contributing to the surface tension decrease per single solute molecule.

The surface density of solute molecules N is equal to Γ for most organic molecules because most of the excess molecules are expected to be in a nanometer region of the surface although, strictly speaking, the definitions of N and Γ differ. Generally, for water-soluble molecules, the Langmuir isotherm given as

$$\frac{1}{\theta} = 1 + \frac{1}{K_{ad}C}, \quad (3)$$

provides a good approximation for the relation between $N=N_{max}\theta$ and C, where θ is the surface coverage, K_{ad} is the adsorption constant, and N_{max} is the maximum value of surface density. Assuming the Langmuir adsorption isotherm, we get

$$\gamma = \gamma_w - vRTN_{\max}\ln(1+K_{ad}C), \quad (4)$$

where γ_w is the surface tension of pure water.

The typical relation between the concentration and surface density is shown in Fig. 2 for two types of rhodamine dyes, estimated from the surface tension-dependence on the bulk concentration using Eq. 4. It is evident that the surface density of an adsorbed solute molecule saturates at a specific concentration. Applicable concentration ranges of a variety of methods are also indicated (*vide infra*).

Surface tension measurements are valuable because the surface density of adsorbed solute molecules can be estimated through them. However, a molecular-scale view of the interface is, unfortunately, not easy to obtain; this is especially true for a condition with low adsorption coverage.

1.3. Interface-selective spectroscopic methods

Interface-selective spectroscopic methods have been applied to provide a variety of information on the solute molecules adsorbed at the water surface. Every interaction between light and surface molecules can be utilized to observe molecules at the interface, as shown in Fig. 3.

Linear spectroscopic methods, such as reflection spectroscopy, including Brewster angle microscopy (Hoenig and Moebius, 1991; Lheveder et al., 2000), and fluorescence spectroscopy, including confocal fluorescence microscopy (Li et al., 1998a; 1998b; Zheng et al., 2000; 2001a; 2001b; 2004), are general and powerful. Nonlinear spectroscopic methods, such as resonance optical second harmonic generation (SHG) (Benjamin, 2006; Shen, 1989; Eisenthal, 1992; Zhao et al., 1990; Slyadneva et al., 1999; 2003; Tsukanova et al., 2000) and vibrational sum-frequency generation (Shen et al., 2006; Gopalakrishnan et al., 2006; Perry et al. 2006), are powerful tools for the surface selective observation of molecular electronic and vibrational states, respectively. However, it is often the case that their sensitivity to detect solute molecules adsorbed at the water surface is not sufficient, especially when the surface coverage is less than 5 % of the monolayer coverage.

The applicable concentration ranges of a variety of methods are summarized in Fig. 2; the findings in this figure are based solely on our experience and are one of the guidelines. Of course, the range depends on the target molecules and experimental conditions. However, among a variety of spectroscopic methods for observing molecules at the air-water interface, the photoionization method surely has good potential to detect adsorbed solute molecules with surface selectivity and sensitivity. Only the fluorescence detection of the surface-adsorbed molecules is highly sensitive. When a confocal fluorescence microscopy is used, surface-selective detection of adsorbed dye molecules is possible up to a surface coverage of 10^{-6} level even if the dye molecule is water-

soluble. However, under a high concentration condition, surface selectivity is lost because the ratio of surface-adsorbed to bulk molecules decreases.

1.4. Photoionization of molecules at the water surface

When photo-emitted electrons from the molecules at the water surface are collected in the upper gas phase, as in the total current yield detection method used in x-ray spectroscopy, the photoionization current flowing from the solution to the ground reflects the photoionization of molecules only at the surface (Fig. 4).

The signal intensity Q of the photoionization current for the m-photon process is described as

$$Q = AI^m \left[\eta_{surf}\sigma_{surf}N + \eta_{bulk}\sigma_{bulk}\int_0^\infty dz \int_0^{\pi/2} d\varphi \{C(z)\sin\varphi \exp(-z/\lambda\cos\varphi)\} \right], \qquad (5)$$

where A is a proportionality constant; I is the pump pulse energy; η_{surf} and η_{bulk} are the effective detection efficiencies of photoemitted electrons from the dye molecules at the surface and in the bulk solution, respectively; σ_{surf} and σ_{bulk} are the photoionization cross sections of the dye molecules at the surface and in the bulk solution, respectively; N is the surface density of the dye molecules; C(z) is the dye concentration depending on depth z from the surface; λ is the escape length of the photoelectrons from the bulk solution, which has been considered to be a few nanometer for electrons (<1 eV) in water (Jo and White, 1991); φ is the angle between the surface normal and the direction of initially emitted electrons. If the bulk concentration is depth-independent, as $C(z)=C$, the double integral in Eq. 5 equals $C\lambda/2$. The small escape depth ensures surface selectivity.

When the Langmuir adsorption isotherm (Eq. 3) is applicable to describe the adsorption of dye molecules at the water surface, a relation between N and C is given by

$$N = N_{max}K_{ad}C/(1+K_{ad}C), \qquad (6)$$

whereN_{max} is the maximum surface density of dye molecules so that surface coverage is $\theta = N/N_{max}$ and K_{ad} is the adsorption equilibrium constant. For dye molecules with surface activity, N is much larger than $C\lambda$ because λ is as small as a few nanometers. Then, we can ignore the second term in the right-hand side of Eq. 5, and the expression of the concentration-dependent photoionization signal intensity for the solution surface observation is given as

$$Q = Q_{max}K_{ad}C/(1+K_{ad}C), \qquad (7)$$

where $Q_{max} = AI^m \eta_{surf} \sigma_{surf} N_{max}$ is the signal intensity at the high concentration limit.

Photoionization phenomena in the gas and condensed phases as well as at the surface have been investigated from a variety of viewpoints, such as chemical physics, physical chemistry, biological chemistry, environmental science, and solar energy conversion (Hatano, 1999; 2001a; 2001b; Ogawa, 1999; Kouchi and Hatano, 2004). Light sources used are conventional vacuum ultraviolet light, synchrotron radiation, and laser.

Vacuum ultraviolet light with photon energy over the ionization potential of a molecule makes the molecule ionized via a one-photon process. A pulsed laser, which generates a light beam of a large photon flux, easily makes a molecule ionized through a multi-photon ionization (MPI) process. Resonant MPI measurements have good sensitivity, wide applicability and, species selectivity; for these reasons, they have been selected as a profitable analytical method.

Photoionization of the water-soluble molecules adsorbed at the aqueous solution surface has been studied (Watanabe et al., 1980; 1983; 1998; Watanabe, 1994; 2006; Winter and Faubel, 2006) because there is a wide variety of surface-active molecules and their adsorption behavior has great importance in physical chemistry, biochemistry, environmental chemistry, and technology. However, it is not always apparent how much the photoionization process is affected by the interaction of the solute with the solvent molecules, how far the solute molecule are from the surface, or how long a molecules stays at the surface.

2. Experimental setups

2.1. Photoionization current spectra of molecules at the water surface

A typical experimental setup for the measurements of photoionization current spectra is illustrated in Fig. 5 (Ogawa et al., 1999; Inoue et al., 1998; Seno et al., 2002). The monochromated synchrotron light (3.5-9.2 eV) was obtained from the beamline 1B at the Ultraviolet Synchrotron Orbital Radiation (UVSOR) facility of Institute for Molecular Sciences (Okazaki, Japan) with a Seya-Namioka monochromator. The light was emitted from the end chamber of the beamline to the He-purged cell through an MgF_2 window. A quartz plate was inserted, if necessary, to cut high-energy photons caused by higher-order diffraction from the grating.

The emitted light was reflected on an Al mirror and vertically irradiated on the aqueous solution surface through a Cu-mesh electrode. The electrode was set at 5 mm above the liquid surface and high voltage (400-500 V) was applied to the electrode so that emitted electrons were collected, for which bias-dependence was checked to collect electrons as much as possible with no abrupt

discharge. The photocurrent (~100 fA) was measured with a picoammeter (Model 617, Keithley). The incident photon intensity was monitored by measuring the fluorescence intensity from a sodium salicylate plate with a photomultiplier tube (1P28, Hamamatsu Photonics).

A sample of aqueous solution was poured in a vessel made of platinum (30 mm diameter, 0.6 cm depth, and 7.07 cm^2 surface area) or stainless steel (34 mm diameter, 0.6 cm depth, and 9.08 cm^2 surface area) and set on an electrode in the cell box. The typical volume of a sample solution was 4 mL.

2.2. Laser multi-photon ionization current of molecules at the water surface

A typical experimental apparatus for the multi-photon ionization experiments for observing molecules at the water surface is shown below (Masuda et al., 1993; Inoue et. al., 1994; Chen et al., 1994; Ogawa et al., 1994a; 1994b). The third harmonic of Nd: yttrium aluminum garnet laser (Minilite Mini Ii, Continuum; wavelength, 355 nm; pulse duration, 4 ns; pulse energy, 10 mJ/pulse) was operated at a repetition rate of 2 Hz. After the pulse energy was adjusted to a certain value less than 0.5 mJ/pulse with a set of a half-wave plate and a glass plate, the laser beam was focused softly with a quartz lens (focal length, 300 mm) on the liquid solution surface at an incident angle of 84°. The polarization plane of the laser beam was controlled with a half-wave plate.

The 4.0 mL sample solution was poured into a stainless steel vessel (34 mm diameter, 0.6 cm depth, 9.08 cm^2 surface area) and set on an electrode in a cell box purged with nitrogen gas, as shown in the inset of Fig. 6 (left). Another disk electrode (12 mm diameter) was placed 10 mm above the solution surface and positively biased at 2.0 kV with a high-voltage power supply (C3350, Hamamatsu). The photocurrent fed from the sample vessel to a current amplifier (428, Keithley; gain, 107 V/A) connected to the ground was measured with a digital oscilloscope (DCS-8200, Kenwood). The signal was accumulated for 64 pulses of the laser. Figure 6 (left) shows a typical time profile of laser two-photon ionization current measured for an aqueous solution of rhodamine B chloride (RhB). The peak current or charge, determined as the time-integrated current, was used as the ionization signal intensity. Generally, no significant difference between the peak current and the charge was found when analyzing the photoionization signal.

Figure 6 (right) shows the pump pulse-energy dependence of the ionization current amplitude of an aqueous solution of RhB. The photoionization signal intensity was quadratically proportional to the laser pulse energy for every concentration investigated regardless of the polarization of the excitation laser. Similar results were obtained for rhodamine 6G chloride (R6G). The photoionization of the rhodamine molecules adsorbed on the water surface in a two-photon process under the excitation wavelength of 355 nm was confirmed. This is reasonable because the photon energy at 355 nm is 3.5 eV and the

photoionization threshold energy of RhB and R6G on the water surface has been reported to be 5.6 eV (Seno et al., 2002). The quadratic dependence shows that the space charge effect is not significant under the experimental conditions and the signal intensity reflects the number of photo-ionized molecules.

2.3. Laser second harmonic generation and surface tension measurements

Second harmonic generation measurements were carried out with an experimental setup described elsewhere (Slyadneva et al., 1999; 2003; Tsukanova et al., 2000). Briefly, a frequency-doubled beam of a pulsed Nd^{3+}: yttrium aluminum garnet laser (PY61, Continuum; wavelength, 532 nm; pulse duration, 40 ps; repetition rate, 10 Hz; maximum pulse energy, 30 mJ/pulse), whose polarization plane was rotated by a half-wave plate to obtain an s- or a p-polarized beam, was softly focused by a quartz lens (focus length 90 cm) at the sample surface, resulting in a beam waist area of 0.25 cm^2. The incident angle was 45° from the surface normal. The energy density per pulse at the surface was 2 mJ/cm^2. The SHG light reflected from the solution surface was separated from the incident laser beam by optical cut-off and band-pass filters and detected with a photomultiplier tube (R585, Hamamatsu). The signal intensity was recorded with a digital oscilloscope (TDS 380, Tektronix). The SHG signal for each measurement under condition of a fixed concentration was averaged over two minutes.

A similar expression to Eq. 7 is obtained for the case of SHG measurements. If it is assumed that the SHG signal is quadratically proportional to the number density of dye molecules at the surface, the SHG signal intensity S is given as

$$S = S_{max}\left[K_{ad}C/(1+K_{ad}C)\right]^2 + S_w, \qquad (8)$$

where S_{max} is the signal intensity at a high concentration limit and S_w is the SHG signal intensity of the water surface. Here, we simply add S_w because SHG from the water surface is non-resonant while SHG from the dye molecules at the water surface is resonant at 532 nm; thus, a $\pi/2$-phase difference is roughly expected.

The surface tension of aqueous solutions of rhodamine dye was measured with a surface-pressure meter (Model HMB, Kyowakaimen) of the Wilhelmy type.

3. Photoionization spectra and photoionization threshold of molecules at the water surface

3.1. Photoionization current spectra of molecules at the water surface

Photocurrent spectra at the surface of both pure water and the aqueous solutions of 1-aminopyrene are shown in Fig. 7, in which the photocurrents are normalized with the ring current of the synchrotron orbital. No significant photocurrents for the surface of pure water and buffer solutions are detected. Thus, the photocurrents for the surfaces of the 1-aminopyrene aqueous solutions are successfully measured for two pH values of the solution. The current shows increases with the photon energy in the region above the photoionization thresholds: the photocurrent shows a similar threshold behavior to that of the bulk solution. Similar spectra are observed for a variety of molecules adsorbed on the water surface.

It is known that the photocurrent, I, near the photoionization threshold, E_{th}, can be represented with an empirical power law (Holroyd et al., 1983; Hoffman and Albrecht, 1991),

$$S = \sum S_i \left(h\nu - E_{th}^{(i)} \right)^n \qquad \text{for} \quad h\nu > E_{th}^{(i)}, \tag{9}$$

where $E_{th}^{(i)}$ is the threshold energy of photoionization for the i-th component, $h\nu$ is the photon energy, and n is an exponent representing the power law with respect to the excess energy $h\nu$-$E_{th}^{(i)}$. The summation of the number of ionization transitions should be conducted.

The photocurrent spectra of 1-aminopyrene at the water surface in Fig. 7 show positive, although not strong, evidence of pH dependence. Both changes in intensity and a small shift in photoionization thresholds are observed (*vide infra*). The spectral shape also changes slightly: a shoulder at 6.1 eV is observed at pH 7.02. It is reasonable because 1-aminopyrene at pH 7.02 has a different chemical form (neutral) from that at pH 1.05 (cationic). However, pyrenebutyric acid and pyrenehexadecanoic acid show pH-independent spectral shapes although the chemical forms are neutral at pH 3.11 and anionic at pH 11.19 while small shifts in photoionization thresholds are observed (*vide infra*). The signal intensity of pyrenehexadecanoic acid is pH-independent. This suggests that solubility might be important for changes in spectral shapes to take place.

A large pH-dependent change in spectral shape is observed for R6G, as shown in Fig. 8. Apparently, the spectral shape at pH 1 is different from those under the other pH conditions although it is known that R6G in a bulk aqueous solution always has a cationic form for these pH ranges (Zheng et al 2004). The cause of the pH-dependent changes in spectral shape has not been specified.

Unfortunately, it is not easy to discuss the spectral shapes; therefore, at the present stage, the photoionization threshold is the only good indicator of photoionization spectra for understanding the state of adsorbed solute molecules. In Section 3.3, the photoionization-threshold dependence on subphase pH is discussed.

3.2. Determination of the photoionization threshold

The empirical relation in Eq. 9 has been generally used to determine photoionization thresholds. Some problems in determining the photoionization thresholds using a fitting procedure are represented in Fig. 9.

First of all, the validity of Eq. 9 is not self-evident and careful consideration is required to adapt the value of the exponent n (Hoffman and Albrecht, 1991). It is not simple to determine threshold energy E_{th} and exponent n at the same time with an experimentally obtained photoionization spectrum even if a single component with one ionization threshold is assumed. Furthermore, the number of ionization transitions is generally unknown for the medium-sized molecules that we are interested in, and a single species of molecule may have more than one chemical form at the water surface.

Figure 9 shows the results of fitting experimental data to the empirical equation. As shown in Fig. 9a, for the single component analysis, there are small fitting errors near the threshold energy, independently of the exponent value; a double component fitting gives better results although there is no reliable explanation for the components being double. What is important is that the threshold energy systematically depends on the exponent values, as shown in Fig. 9b, for both single and double component fittings. It is concluded that the accuracy of the determined ionization threshold is influenced by the exponent value used.

It is true that the summation of the residual errors in the fitting has a minimum, as shown in Figs. 9c and 9d, but the position of the minima is not on $n = 2.5$ or 3.5, which is the value typically used as the exponent value. In summary, for the determination of ionization thresholds, it is realistic and effective to assume the number of components and the exponent to fixed values, respectively, but accuracy limitations should be taken into account.

3.3. Photoionization thresholds of molecules at the water surface

Determined photoionization thresholds (eV) of chemicals on the water surface are summarized in Table 1 for a few pH values of the water subphase. Reference values of the ionization potential (Farrell and Newton, 1965; Timoshenko et al., 1981) are given below the table. In the analysis, the exponent of 2.5 is used, and a single component for the ionization threshold is assumed so that some systematic errors could be included in the threshold energy.

The photoionization threshold E_{th} of a solute in a bulk solution is related to the ionization potential at the gas phase, IP, as follows (Holroyd et al., 1983),

$$E_{th} = IP + P^{+} + V_0, \tag{10}$$

where P^+ is the polarization energy of the resultant positive ion and V_0 is the electron affinity of the solvent. The polarization energy P^+ can be calculated with Born's equation (Born, 1920),

$$P^+ = \frac{-e^2}{8\pi\varepsilon_0 r}\left(1-\frac{1}{\varepsilon_r}\right), \tag{11}$$

where e is the elemental charge of electron, ε_0 is the dielectric constant of vacuum, r is an effective radius of the ion, and ε_r is the relative dielectric constant of the medium. For the ionization of molecules at the liquid surface, V_0 in Eq. 10 seems negligible because the photoelectron is directly emitted to the gas phase.

The experimental value of P^+ for RhB at the aqueous solution surface is -1.1 eV. It is suggested that the probe molecule for photoionization is positioned in a space where the photogenerated positive ion can sufficiently interact with the solvent water molecules. On the other hand, the value of P^+ in the aqueous solution estimated with Eq. 11 is -0.5 eV, where the effective radius r of the RhB positive ion is roughly estimated to be 0.6 nm with Corey-Pauling model (Koltun, 1965) of the RhB molecule. The large P^+ value experimentally observed suggests that V_0 cannot be ignored even at the surface or the effective radius of resultant positive RhB ion is smaller than 0.6 nm.

As for the pH-dependence, shown in Table 1, the tendencies observed for pyrene derivatives are summarized as follows: more positively charged forms tend to have higher thresholds; the threshold downshifts 0.20-0.27 eV per electron charge; and the shifts of insoluble species (pyrenehexadecanoic acid) and less soluble ones (pyrenebutyric acid) are smaller than those of soluble ones (aminopyrene). These results are not surprising when the charge density of the pyrene unit is considered. The small shift for insoluble species could come from immovability in the depth position, indicating a constant degree of solvation between charged and neutral forms.

Rhodamine 6G (soluble species) has the same chemical forms in the bulk aqueous solution throughout the pH range investigated (Zheng et al 2004), but the threshold shift is observed: a lower pH results in a higher threshold. The degree of protonation seems to cause the results. At pH 1, a different chemical form from that at a higher pH is expected for R6G only at the water surface. This is already suggested in Fig. 8. Although the expected surface-specific chemical form is not identified, a similar proposal has been reported in a confocal fluorescence study of R6G molecules at the water surface (Zheng et al 2004).

3.4. Photoionization of rhodamine B at the water surface under self-assembled layer

Photoelectron emission from a liquid solution surface covered with a self-assembled layer of aliphatic acid has been investigated (Ishioka et al., 2003; 2004). The sample solutions investigated were composed of a surface-active dye (RhB, 10 μM), a buffer electrolyte (HCl, pH 1.0), and water. The aqueous solution surface was modified with arachidic acid ($C_{19}H_{39}COOH$) by spreading as a benzene solution. The added amount was approximately within two monolayers at the maximum surface density, which is calculated by the assumption that a close-packed layer was formed on the aqueous solution surface.

Similar shapes of photoionization spectra were observed for all the surface density of arachidic acid: no significant change in photoionization thresholds was observed while the signal intensities were increased or decreased. Figure 10 (left) shows the plot of the photocurrent intensity at 6.67 eV measured by single-photon ionization against the added amount of arachidic acid. The current intensity increases remarkably when a small amount of arachidic acid is added (~0.2 monolayer) and then decreases to a constant value above the monolayer formation level. These experimental results cannot be explained by a simple model based on uniform monolayer formation and simple electron scattering through the aliphatic monolayer because this model needs a monotonous decrease of the photoionization current upon film formation.

Figure 10 (right) shows the same experiment as described above except that the measurement was conducted by laser two-photon ionization under a beam-focusing condition. The pulse-to-pulse deviation of the signal intensity is remarkable at the concentration range of the photocurrent increase. The increased fluctuation suggests that a small domain formed by the arachidic acid layers has a comparable size to that of the focused area (10-100 μm). Aggregate formation and the accumulation of dyes around the aggregates are the most probable explanations for the enhancement of the photoionization current by arachidic acid addition.

A similar experiment was performed with a series of aliphatic acids having different CH-chain lengths. Details of the analyses will be published elsewhere.

4. Photoionization-current dependence on the surface density of solute molecules and effect of incident light polarization

4.1. Concentration dependence of surface-selective signals of rhodamine dyes at the water surface: Laser multiphoton ionization and second harmonic generation studies

Resonant laser multiphoton ionization is superior to one-photon ionization because it has species selectivity as well as surface selectivity. Resonant second harmonic generation has both species selectivity and surface selectivity as well.

Data given in this section are based on measurements of laser multiphoton ionization, second harmonic generation, and surface tension (Seno et al., 2001; Harata et al., 2009).

The concentration dependences of the photoionization charge of aqueous solutions of RhB and R6G are shown in Fig. 11 (left). The intensity of the signal generated with s- and p-polarized laser light excitation at 355 nm is plotted. All the data show the saturation behavior of the photoionization signal at high-concentration regions, as expected from Eq. 7. The curves are fitting results of the experimental data to the Langmuir isotherm, for which the fitting parameters of K_{ad} (M^{-1}) and Q_{max} (fC) are summarized in Table 2. Equation 7 represents the experimental data well. The results suggest that rhodamine molecules adsorbed at the water surface are selectively detected and that the photoionization signal from rhodamine molecules in the bulk solution is negligible, as is that from water molecules. As the magnitudes of Q_{max} in Table 2 demonstrate, the photoionization signal of RhB is larger for s-polarized than for p-polarized excitation, while R6G shows the reverse order. It is suggested that the transition moment of the two-photon photoionization (TPI) is relatively parallel and perpendicular to the water surface for RhB and R6G, respectively. The polarization dependence of K_{ad} observed for both RhB and R6G suggests that σ_{surf} and/or η_{surf} varies with the bulk concentration, meaning that the molecular orientation at the surface changes with the bulk concentration. Details of the values K_{ad} and Q_{max} are discussed later.

Figure 11 (right) shows the concentration dependence of the SHG signal intensity from the surface of aqueous solutions of rhodamine dyes when s- or p-polarized laser light at 532 nm excites the surfaces of aqueous solutions of RhB and R6G. All the data show the saturation behavior of the SHG signal at high-concentration regions, as expected from Eq. 8. The curves are fitting results of the experimental data to Eq. 8, for which the fitting parameters of K_{ad} (M^{-1}) and S_{max} (arb. units) are listed in Table 2. Equation 8 represents the experimental data well, as shown in Fig. 11 (left); however, K_{ad} of R6G is one order of magnitude smaller than that obtained in photoionization experiments. Moreover, the polarization dependence of S_{max} is quite different from that of the photoionization measurements. Details of the values K_{ad} and S_{max} are discussed later.

4.2. Measurements of surface tension and ultraviolet-visible absorption spectra

Surface tension and ultraviolet absorption measurements provide important reference data for following discussion on solute dye molecules adsorbed at the water surface (Seno et al., 2002; Harata et al., 2009).

The dependence of the surface tension of the rhodamine solutions on the concentration is shown in Fig. 12 (left). The surface tension of each rhodamine aqueous solution decreases with the bulk concentration. This clearly indicates

that each rhodamine molecule is positively adsorbed to the water surface. The curves are fitting results of the experimental data to Eq. 4. In Table 3, the fitting parameters K_{ad} (M^{-1}) and N_{max} (mol/m^2) are summarized for each rhodamine dye with the specific molecular area A_{min} (nm^2/molecule) corresponding to N_{max}. In calculating N_{max}, $\nu=1$ is assumed. At a neutral pH, the principal chemical forms of RhB, R6G, and Rh101 are zwitterion, cation, and zwitterion, respectively. The assumption $\nu=1$ means that the surface activity of protons, chloride ions, and perchloride ions is neglected.

It has been reported that the surface pressure-area isotherm of dioctadecyl-rhodamine B (RhB-based water-insoluble rhodamine dye having two long hydrocarbon chains on two monoethylamino groups) shows a collapse pressure at 0.26 nm^2/molecule (Slyadneva et al., 2001). This value is as small as 10, 1.6, and 0.68 % of A_{min} of RhB, R6G, and Rh101, respectively. The fact indicates that each rhodamine dye, especially R6G, has enough space at the water surface even when adsorption is saturated. Strong interaction between dye molecules at the water surface could be expected.

The ultraviolet absorption spectra of rhodamine dyes in Fig. 12 (right) shows that multiphoton ionization at 355nm of each dye investigated is under a resonant condition. Although there is a possibility that the absorption peak of the rhodamine dyes at the water surface shifts from those of bulk aqueous solution, we disregard the possibility because no large spectral shift is expected.

In discussing molecular orientation, it is important as well as useful to consider the direction of the effective transition moment for TPI of rhodamine dyes because of the complexity of the two-photon process. All the rhodamine dyes used have an absorption peak around 540 nm, attributed to a transition from the ground state to the first singlet excitation state S_1, whose transition dipole moment is nearly parallel to the xanthene ring (x-direction in Fig. 8) (Jakobi and Kuhn, 1962; Peterson and Harris, 1989; Drexhage, 1997). The second singlet excitation state S_2 lies at around 350 nm, and the transition dipole moment is nearly perpendicular to the xanthene ring (y-direction in Fig. 7) (Jakobi and Kuhn, 1962; Peterson and Harris, 1989; Drexhage, 1997). The excitation wavelength of 355 nm in the photoionization experiment is resonant with the transition to the second singlet excitation state S_2.

The resonant two-photon photoionization process may be caused by both a simultaneous two-photon process and a stepwise two-photon process, and the contributing ratio of both processes depends on the intensity and pulse width of the excitation laser. In the simultaneous process, two-photon absorption of the ground state molecules directly into a pre-ionization state via the intermediate S_2 state should be considered. In the stepwise process, three processes, i.e., photoexcitation to S_2, relaxation from S_2 to S_1, and photoionization from S_1, should be taken into consideration in combination. Unfortunately, little is known of the directions of the transition moments for the simultaneous two-photon absorption and stepwise S_2 absorption as well as of their contributing

ratio. Strictly speaking, we cannot identify the direction of the transition moment for the TPI of the rhodamine dyes. However, a simple assumption can be considered: the direction is the same as that of resonance photo-absorption, namely, y-direction. This might be reasonable if the resonance process dominates the two-photon absorption in the simultaneous process and if the transition from S_2 to the pre-ionization state does not have large anisotropy.

A similar discussion can be made for the direction of the transition moment for SHG. The direction is assumed to be parallel to that of the resonance photo-absorption, namely, the x-direction. Under these assumptions, we could determine the averaged direction of adsorbed rhodamine molecules at the water surface. Such a discussion has been reported for 1-pyrenehexadecanoic acid on the water surface (Sato et al., 2001).

4.3. Concentration-dependent orientation of dye molecule at the water surface

Figure 13 (left) shows the dependence of the photoionization signal intensity $I(\theta)$ on the polarization angle θ of the excitation laser with 84° of the incident angle (Seno et al., 2001; Harata et al., 2009). Four different-concentration data sets are shown of aqueous solutions of each rhodamine dye. θ=0° and θ=90° correspond to p- and s-polarized light, respectively: $I_p = I(\theta=0°)$ and $I_s = I(\theta=90°)$. The curves are the fitting results of the experimental data to sinusoidal functions. As seen, this function describes each of the polarization dependences well. The arrows in Fig. 13 (left) indicate the order of the sample concentrations noted on the right-hand side. It is notable that the polarization dependence does not monotonically change with the concentration.

In Fig. 13 (right), the ratio I_p/I_s of the photoionization signal intensity, representing the polarization dependence, is plotted as a function of the surface excess for aqueous solutions of RhB and R6G. The surface excess is calculated with the concentration of the solutions using the adsorption properties listed in Table 3. Notable features are that for each rhodamine dye, the I_p/I_s values show a maximum or minimum around a point where the surface excess is just saturated and the I_p/I_s values decrease or increase gradually even under a much lower surface excess condition than the extreme point. The former indicates that the direction of the effective transition moment changes with the surface excess, and the latter means that molecules on the water surface significantly interact with each other even when they have enough free area for moving on the surface.

4.4. Effective adsorption equilibrium constants

It is not necessary for the adsorption equilibrium constants (effective adsorption equilibrium constants), experimentally determined with a variety of methods, to agree with each other because different types of interactions are used for these measurements. Surface tension measurements providing surface

excess are based on the thermodynamic equilibrium, for which the spatial distributions of the concentration and orientation of molecules in the depth direction are left out of consideration. On the other hand, photoionization and SHG signals depend on the spatial distribution of molecules. As for photoemission, when the photoemitting groups of the dye molecules are positioned as upper the water surface, a larger the photoionization signal is detected because of a smaller disturbance from water molecule. As for SHG, when photoabsorbing chromospheres of the dye molecules are closer positioned to the air-water boundary and are better oriented at the boundary, a larger resonant-SHG signal is detected because of a larger second-order nonlinear susceptibility. Consequently, the effective adsorption equilibrium constants determined with a variety of methods and experimental conditions reflect the state and behavior of molecules at the water surface.

As summarized in Tables 2 and 3, the adsorption equilibrium constants K_{ad} of RhB determined by measurements of the surface tension, TPI and SHG, have the same order of magnitude but K_{ad} by TPI and SHG is 69 and 47 % for s-polarized excitation (84 and 45 % for p-polarized excitation) of that by the surface tension, respectively (Seno et al., 2001; Harata et al., 2009). The results have meaningful implications: the surface density of RhB molecules increases as the bulk concentration increases even after surface excess saturation, suggesting the existence of a concentration gradient under the surface whose magnitude depends on the concentration, and the orientation of dye molecules at the water surface depends on the bulk concentration, as discussed before. Figure 14 (left) shows the dependence of the photoionization charge on the surface excess of RhB on the water surface. Photoionization charges are larger than expected from a linear relation between the surface excess and the charges both for s- and p-polarized excitation. It is qualitatively explainable that, as bulk concentration increases, the RhB molecules rise up and adhere closer to the gas phase.

The difference between the determined K_{ad} values of R6G is more significant than RhB: K_{ad} by TPI and SHG is 36 and 2.1 % for s-polarized excitation (47 and 3.8 % for p-polarized excitation) of that by surface tension, respectively. Figure 14 (right) shows the dependence of photoionization charge on the surface excess of R6G on the water surface. Photoionization charges seem quadratically dependent on the surface excess and are much larger than expected from a linear relation both for s- and p-polarized excitation. The results can be explained by the same mechanism as RhB, although the concentration-dependent changes of the concentration-gradient and molecular orientation are large for R6G.

4.5. Rhodamine dyes at the water surface

A rough sketch, based on the discussion above concerning the rhodamine dyes adsorbed at the water surface, is shown in Fig. 15 (Harata, 2003). As the time and ensemble average, RhB and R6G at the water surface have different orientations. The concentration-dependent behavior, indicated by arrows in the figure, is also different. Even if two dye molecules are far apart from each other at the water surface, some effective interaction is expected. It is noteworthy, of course, that further discussion along with precise experiments and analyses is required even for the time- and ensemble-averaged view of surface-adsorbed molecules. A dynamic view with fluctuation of the orientation and three-dimensional position of molecules and with adsorption-desorption behavior will be presented in further studies.

5. Detection and monitoring of molecules at the water surface

5.1. Detection limit of molecules at the water surface by photoionization measurements

Laser-based spectroscopic techniques generally provide high sensitivity in molecule detection even for molecules adsorbed at the water surface. However, when surface-selective detection is required, as in the case of detecting adsorbed liquid-soluble molecules on the liquid solution surface, three main techniques are currently available: confocal laser fluorescence, SHG, and TPI. For non- or less-fluorescent molecules, there are two techniques. Second harmonic generation spectroscopy, the most popular technique for studying molecules on a liquid surface, is particularly sensitive to the first layer of the liquid surface. The second one is laser two-photon ionization spectroscopy, which is sensitive for detection of probe molecules both in a bulk solution (Voigtman et al., 1981; 1982; Yamada et al., 1982; 1983; 1986: Ogawa et al., 1992a; 1995) and on the surface of a solution (Masuda et al., 1993; Inoue et. al., 1994; Chen et al., 1994; Ogawa et al., 1994a; 1994b; Gridin et al., 1998) or metal (Ogawa et al., 1992b). The sensitivities of these two techniques are, however, different, as shown in Fig. 2. The typical detection limit of a solute molecule with the TPI technique was 0.25 pmol/cm^2 (Ogawa et al., 1992b), while that with the SHG technique was 5.0 pmol/cm^2 (Inoue et al., 1995).

It is important to estimate the detection limit of a target molecule theoretically or empirically. The detection limit of molecules at the water surface by TPI measurements depends on the properties of target molecules as well as the experimental conditions, which include the absorption coefficient ε at the excitation wavelength, the photoionization threshold E_{th}, the energy of the first excited singlet state E_{S1}, and the adsorption coefficient K_{ad}. It is natural to assume that the detection limit expressed as the bulk concentration is inversely proportional to $\varepsilon E_{excess}{}^{n} K_{ad}$, where n is the exponent given in Eq. 9 and E_{excess} is

excess energy in photoionization relating to photon energy $h\nu$. For a stepwise TPI process, $E_{excess} = (E_{S_1} + h\nu) - E_{th}$, and $E_{excess} = 2h\nu - E_{th}$ for simultaneous TPI. Even if well-defined experimental conditions are adjusted, it is often the case that some of the properties of the target molecules are unknown. Especially, few reference values are available for K_{ad} of targets. It is not easy to obtain solubility data either. To roughly evaluate K_{ad}, *n*-octanol and the water partition coefficient *P*(o/w) may be useful because *P*(o/w) is easily estimated as an indicator of water solubility.

Table 4 is a summary of the detection limits of some chemicals on the aqueous solution surface (Inoue et. al., 1994; Maeda et al., 2005; Maeda, 2006), along with the molecular absorptivity, excess energy, and *n*-octanol and water partition coefficient. As shown, there is no good correlation between the detection limit and ε, E_{th}, or log*P*(o/w), but some tendencies to a higher detection limit are seen for chemicals with higher ε and higher log*P*(o/w). This could be a measure of estimating the detection limit, which may be applicable even for molecules with unknown properties.

5.2. Acid-base equilibrium constant of molecules at the water surface

Two-photon photoionization measurements have been used to determine the acid-base equilibrium constants of the molecules on the water surface and the distribution coefficients of neutral species and ionized species between the surface and bulk water (Sato et al., 2000; 2004). The photoionization signal of 1-aminopyrene (4.0 nmol in the 0.600 mL vessel) on the water surface was measured for aqueous solutions with various pH values. Figure 16 (left) shows the result, in which the ordinate is normalized to the value of the signal for aminopyrene at pH 8 for simplicity. The photoionization signal of aminopyrene on the water surface tends to increase with increasing subphase pH, meaning that the surface concentration of aminopyrene increases with the pH. Although both neutral and ionic forms of aminopyrene may stay in the bulk and on the surface of water in principle, neutral species are expected to prefer to stay on the surface, and the ionic species, in bulk water. This is reasonable because ionic species are more hydrophilic than neutral species. It is natural to assume that signals observed around pH 0-1 are mainly due to cationic species on the water surface and those around pH 6-8 are mainly due to neutral species.

The pH dependence of the photoionization signal can be described with the following equilibrium-constants: the acid-base dissociation constants for solution surface (K_{a_s}) and for bulk solution (K_{a_b}); and the distribution coefficients between the surface and bulk of neutral species (K_{DA}) and cationic species (K_{DHA}) of solute molecules. These constants are defined by

$$K_{a_s} = [A]_s[H^+]_s/[HA^+]_s, \qquad (12a)$$

$$K_{a_b} = [A]_b\,[H^+]_b/[HA^+]_b, \quad (12b)$$

$$K_{DHA} = [HA^+]_s/[HA^+]_b, \quad (12c)$$

$$K_{DA} = [A]_s/[A]_b, \quad (12d)$$

where the subscript s denotes the quantity on the surface and where the surface concentration means an effective concentration within the region of the escape depth of a photoelectron. It is possible that $[H^+]_s$ is different from $[H^+]_b$ due to the existence of a surface charge (Zhao et al., 1990), but, because the absolute number density of the ionized species on the surface is small in this case, the difference in pH between the surface and the bulk is negligible: $[H^+]_s = [H^+]_b$. Among four equilibrium constants, K_{a_b} is estimated with fluorometry of bulk solution to be 3.6±0.1 for aminopyrene (Sato et al., 2004); the distribution coefficients are estimated to be K_{DHA}= 2.5 x 10^{-7} m and K_{DA}= 9.6 x 10^{-7} m by comparison of the photoionization signal intensity of aminopyrene with that of insoluble pyrene derivatives of pyrenehexadecanoic acid.

The observed photoionization signal is proportional to $\eta_A[A]_s+\eta_{HA}[HA^+]_s$, where η_A and η_{HA} are the photoionization efficiencies of neutral and ionized forms of aminopyrene on the water surface, respectively. The ionization efficiencies, η_A and η_{HA}, of neutral forms and ionized forms, respectively, are of critical importance in solving Eqs. 12 (Sato et al., 2000). The ratio, η_{HA}/η_A, is estimated to be 9.4 on the basis of assumption that the ionization efficiency of the two forms is dominated only by a resonant condition, namely, the absorption coefficient at the excitation wavelength (Sato et al., 2004).

With the above consideration, pK_{a_s} is determined to be 2.0. The solid curve in Fig. 16 (left) is theoretically calculated with these equilibrium constants, which agrees well with the experimental data. A decrease in the surface concentration with decreasing pH is attributed to the decrease in neutral species; the neutral form of aminopyrene is more likely to stay on the surface than the ionized form.

A similar analysis was performed for 1-pyrenebutyric acid, as shown in Fig. 16 (right) (Sato et al., 2000). The distribution coefficients for neutral and ionic species are reported to be (5.9±2.8) x 10^{-2} m and (4.82±0.1) x 10^{-5} m, respectively, and pK_{a_s} is 7.85±0.13. The acid-Base equilibrium constants of adsorbed molecules are quite different from those in bulk solutions, even under the low surface-density conditions.

5.3. Monitoring of volatile molecules spread on the water surface

The adsorption-desorption dynamics of molecules between liquid and gas phases are of fundamental and practical importance. Desorption of volatile molecules from the liquid to gas phase was investigated with ultraviolet single-photon photoionization measurements (Harata et al., 2002). Figure 17 shows the time-dependent photoionization spectra of the water surface after spreading 10 μL p-xylene on a 9.08 cm^2 area. The photoionization signal intensity decreased with time. It changed rapidly in the initial 12 min and continued to decrease gradually over 90 min. This reflects the desorption of p-xylene from the water surface. Although p-xylene in the gas phase could contribute to the ionization signal in this case, the amount of molecules in gas phase is expected to be much smaller than that at the water surface. Unfortunately, the spectral shapes in Fig. 17 are strongly influenced by water vapor, and the complementation for the real photoionization spectra of p-xylene at the water surface is not an easy task because an estimation of light intensity at the water surface is required. However, monitoring could be performed.

In Fig. 18, time traces are shown of the photoionization current at the water surface after 3 μL benzene was spread over a 9.08 cm^2 area. The responses of the initial 5 minutes are dependent on the excitation wavelength, but it is clearly evident that the signal caused by the spread benzene remains on the water surface for 2 hours after spreading.

Benzene is the most preferable solvent for spreading organic molecules on the water surface because it has an appropriate balance of surface tension and interface tension (vs. water) to expand a benzene solution rapidly over the water surface. Thus, benzene has been used as a spreading solvent in a monolayer film formation, such as the Langmuir-Blodgett technique, even though it is a toxic solvent. On the basis of surface tension measurements, benzene is assumed to evaporate within 5 minutes after a base is spread (Pagano and Gershfeld, 1972; Birdi 1999, p. 37). The result in Fig. 18 disproves common sense.

6. Summary

In this chapter, we describe the photoionization measurements of solute molecules adsorbed at the water surface. The molecular-level understanding of molecules at the water surface is still developing, mainly due to lack in methodology for observations with good surface- and species selectivity and sensitivity. Powerful tools for interface selective observation, such as second harmonic generation and sum-frequency generation, sometimes lack sensitivity. The fluorescence measurement of a powerful tool for sensitive observation often suffers from surface selectivity and adaptability to less fluorescent molecules. Thus, a photoionization measurement with moderate sensitivity, fine surface selectivity, and good applicability would be an attractive technique.

Some discussion on photoionization thresholds, polarization- and concentration dependence, and surface molecular monitoring has been presented of surface-adsorbed molecules; however, the details of discussion are still insufficient. Especially, we cannot still experimentally determine the average depth of adsorbed solute molecules, which relates to the degree of hydration of the adsorbed molecules.

Here, we have introduced only a few studies on self-assembled layers on the water surface and no studies on immiscible liquid-liquid interfaces (Tashiro at al., 2003; Inoue et al., 2005). Theoretical studies also provide valuable information (Benjamin, 2006; Perry et al. 2006; Jungwirth and Tobias, 2006b; Mundy and Kuo, 2006; Chang and Dang, 2006; Garret et at al., 2006); thus, a comparison between theory and experiments is essential. The molecular-level understanding of interfaces has attracted increasing attention, and many types of spectroscopic methodologies should be used to enhance such an understanding. Among them, photoionization measurements will provide valuable information.

Acknowledgements

A part of this work was financially supported by a grant from the Global-Center of Excellence in Novel Carbon Resource Sciences, Kyushu University. Authors would like to express their gratitude to Yoshihiko Hatano, professor emeritus of Tokyo Institute of Technology and former professor at Kyushu University, for his participation in helpful discussions.

References

Benjamin, I., 1996. Chemical reactions and solvation at liquid interfaces: a microscopic perspective. Chemical Reviews 96, 1449-1475.
Benjamin, I., 2006. Static and dynamic electronic spectroscopy at liquid interfaces. Chemical Reviews 106, 1212-1233.
Birdi, K. S. (Ed.), 1997. Handbook of Surface and Colloid Chemistry, CRC press, Boca Raton.
Birdi, K. S., 1999. Self-assembly monolayer structures of lipids and macromolecules at interfaces, Kluwer Academic/Plenum Publishers, New York.
Born, M., 1920. Volumes and hydration warmth of ions. Zeitschrift für Physik 1, 45-48.
Chang, T-M., Dang, L. X., 2006. Recent advances in molecular simulations of ion solvation at liquid interfaces. Chemical Reviews 106, 1305-1322.
Chen, H., Inoue, T., Ogawa, T., 1994. Solvents effects in determination of anthracene on solution surfaces by laser two-photon ionization technique. Analytical Chemistry 66, 4150-4153.

Davidovits, P., Kolb, C. E., Williams, L. R., Jayne, J. T., Worsnop, D. R., 2006. Mass accommodation and chemical reactions at gas-liquid interfaces. Chemical Reviews 106, 1323-1354.
Donaldson, D. J., Vaida, V., 2006. The influence of organic films at the air-aqueous boundary on atmospheric processes. Chemical Reviews 106, 1445-1461.
Drexhage, K. H., 1997. Structure and properties of laser dyes. In: Dye Lasers, 2nd Ed., Schäfer F. P. (Ed.), Springer, Berlin, 167.
Eisenthal, K. B., 1992. Equilibrium and dynamic processes at interfaces by second harmonic and sum frequency generation . Annual Review of Physical Chemistry 43, 627-661.
Farrell, P. G., Newton, J., 1965. Ionization potentials of aromatic amines. Journal of Physical Chemistry 69, 3506-3509.
Garret, B. C., Schenter, G. K., Morita, A., 2006. Molecular simulation of the transport of molecules across the liquid/vapor interface of water. Chemical Reviews 106, 1355-1374.
Gopalakrishnan, S., Liu, D., Allen, H. C., 2006. Vibrational spectroscopic studies of aqueous interfaces: salt, acids, bases, and nanodropes. Chemical Reviews 106, 1155-1175.
Gridin, V. V., Litani-Barzilai, I., Kadosh, M., Schechter, I., 1998. Determination of aqueous solubility and surface adsorption of polycyclic aromatic hydrocarbons by laser multiphoton ionization. Analytical Chemistry 70, 2685-2692.
Hatano, Y., 1999. Interaction of vacuum ultraviolet photons with molecules. Formation and dissociation dynamics of molecular superexcited states. Physics Reports 313, 109-169.
Hatano, Y., 2001a. Interaction of VUV photons with molecules - spectroscopy and dynamics of molecular superexcited states. Journal of Electron Spectroscopy and Related Phenomena 119, 107-125.
Hatano, Y., 2001b. Spectroscopy and dynamics of molecular superexcited molecules. In: Sham. T. K. (Ed), Chemical Applications of Synchrotron Radiation World Scientific Publishing Co., Singapore, 55-111.
Harata, A., 2003. Ultrasensitive and ultrafast spectroscopies for investigating dynamic behavior of molecules in a nanospace at interfaces. Housyasen Kagaku 75, 12-19 (in Japanese).
Harata, A., Ishioka, T., Hatano, Y., 2002. Photoionization of molecules adsorbed at the water surface: acidity dependence of photoionization thresholds studied with a synchrotron light source. Abstract of The 1st Saga Synchrotron Light Symposium (SSLS2002, Tosu, Saga, 2002), 21-22.
Harata, A., Seno, K., Slyadneva, O. N., Hatano, Y., 2009. Unpublished results.
Hoenig, D., Moebius, D., 1991. Direct visualization of monolayers at the air-water interface by Brewster angle microscopy. Journal of Physical Chemistry 95, 4590-4592.
Hoffman, G. J., Albrecht, A. C., 1991. Near-threshold photoionization spectra in nonpolar liquids: a geminate pair based model. Journal of Physical Chemistry 95, 2231-2241.

Holroyd, R. A., Preses, J. M., Zevos, N., 1983. Single-photon induced conductivity of solutes in nonpolar solvents. Journal of Chemical Physics 79, 483-487.
Inoue, T., Masuda, K., Nakashima, K., Ogawa, T., 1994. Highly Sensitive Detection of Aromatic Molecules by Laser Two-Photon Ionization on the Surface of Water in Ambient Air. Analytical Chemistry 66, 1012-1014.
Inoue, T., Moriguchi, M., Ogawa, T., 1995. Highly sensitive determination of dye molecules on a surface by the second harmonic generation technique. Analytical Sciences 11, 671-672.
Inoue, T., Sasaki, S., Tokeshi, M., Ogawa, T., 1998. Photoionization threshold of perylene on water surface as measured by synchrotron radiation. Chemistry Letters, 609-610.
Inoue, T., Nishi, H., Kitauira, T., Kurauchi, Y., Ohga, K., 2005. Highly sensitive determination of aromatic molecules in the interface region of an oil/water system using laser two-photon ionization. Bunseki Kagaku 54, 467-471.
Ishioka, T., Harata, A., Hatano, Y., 2003. Photoionization of adsorbed dye below aliphatic acid monolayer at the aqueous solution surface. UVSOR Activity Report 2002, 108-109.
Ishioka, T., Harata, A., 2004. Nonuniform distribution of adsorbed dye at the water surface probed by photoionization methods. UVSOR Activity Report 2003, 54.
Jakobi, H., Kuhn, H., 1962. The orientation of the transition moments of absorption bands of acridinephenazine, phenoxazine, and xanthine dyes from dichroism and fluorescence-polarization studies. Zeitschrift fuer Elektrochemie und Angewandte Physikalische Chemie 66, 46-53.
Jo, S. K., White, J. M., 1991. Low energy (<1 eV) electron transmission through condensed layers of water. Journal of Chemical Physics 94, 5761-5765.
Jungwirth, P., Finlayson-Pitts, B.J., Tobias, D. J., 2006a. Introduction: structure and chemistry at aqueous interfaces. Chemical Reviews 106, 1137-1139.
Jungwirth, P. Tobias, D. J., 2006b. Specific ion effects at air/water interface. Chemical Reviews 106, 1259-1281.
Koltun, W. L., 1965. Precision space-filling atomic models. Biopolymers 3, 665-679.
Kouchi, N., Hatano, Y., 2004. Interaction of photons with molecules: photoabsorption, photoionization and photodissociation. In: Mozumder, A., Hatano, Y. (Eds), Charged Particle and Photon Interactions with Matter: Chemical, Physicochemical, and Biological Consequences with Applications, Marcel Dekker, New York, 105-120.
Li, Y.-Q., Sasaki, S., Inoue, T., Harata, A., Ogawa, T., 1998a. Spatial Imaging Identification in a fiber-bundle confocul Fluorescence microspectrometer. Applied Spectroscopy 52, 1111-1114.
Li, Y.-Q., Slyadnev, M. N., Inoue, T., Harata, A., Ogawa, T., 1998b. Spectral fluctuation and heterogeneous distribution of porphine on a water surface. Langmuir 15, 3035-3037.
Lheveder, C., Meunier, J., Henon, S., 2000. Brewster angle microscopy. Physical Chemistry of Biological Interfaces, 559-575.

Maeda, Y., Isoda (Sato), M., Ishioka, T., Harata, A., 2005. Analysis of environmental chloride and nitride pollutants at the water surface by photoionization methods using laser and synchrotron radiation. Books of Abstracts for 7th Cross Straits Symposium on Material, Energy, and Environmental Sciences (Fukuoka, Japan, 2005), 251-252.
Maeda, Y., 2006. Chemical state analysis of environmental molecules adsorbed at the water surface by using photoionization methods. Master Thesis (Kyushu Univ. 2006), 1-40 (in Japanese).
Masuda, K., Inoue, T., Yasuda, T., Nakashima, K., Ogawa, T., 1993. Highly sensitive detection of pyrene by laser multi-photon ionization on the surface of water. Analytical Sciences 9, 297-298.
Motomura, K., 1978. Thermodynamic studies on adsorption at interfaces. I. General formulation. Journal of Colloid and Interface Science 64, 348-355.
Motomura, K., Iwanaga, S., Hayami, Y., Uryu, S., Matuura, R., 1981. Thermodynamic studies on adsorption at interfaces. IV. Dodecylammonium chloride at water/air interface. Journal of Colloid and Interface Science 80, 32-38.
Mundy, C. J., Kuo, I-F. W.. 2006. First principles approaches to the structure and reactivity of atmospherically relevant aqueous interfaces. Chemical Reviews 106, 1282-1304.
Ogawa. T., 1999. Laser 2-photon ionization in solution and on surface in ambient air: investigations through conductivity measurement. In: Ng. C.-Y. (Ed), Photoionization and Photodetachment, World Scientific Publishing Co., Singapore, 601-633.
Ogawa, T., Chen, H., Masuda, K., Inoue, T., 1994a. Highly sensitive determination of aromatic molecules on the water surface by laser two-photon ionization at 355 nm. Analytical Sciences 10, 219-221.
Ogawa, T., Chen, H., Inoue, T., Nakashima, K., 1994b. Laser two-photon ionization spectrometry and photoionization threshold of perylene on the surface of water. Chemical Physics Letters 229, 328-332.
Ogawa, T., Kise, K., Yasuda, T., Kawazumi, H., Yamada, S., 1992. Trace determination of benzene and aromatic molecules in hexane by laser two-photon ionization. Analytical Chemistry 64, 1217-1220.
Ogawa, T., Sato, M., Tachibana, M., Ideta, K., Inoue, T., Nakashima, K., 1995. Dependence of the laser two-photon ionization signal of anthracene on the electron mobility and the excess energy in non-polar solvents. Analytica Chimica Acta 299, 355-359.
Ogawa, T., Sasaki, S., Tokeshi, M., Inoue, T., Harata, A., 1999. One-Photon `Photoionization Thresholds of Aromatic Molecules at Water/Air Surface. UVSOR Activity Report 1998, 68-69.
Ogawa, T., Yasuda, T., Kawazumi, H., 1992. Laser two-photon ionization detection of aromatic molecules on a metal surface in ambient air. Analytical Chemistry 64, 2615-2617.
Pagano, R. E., Gershfeld, N. L., 1972. Millidyne film balance for measuring intermolecular energies in lipid films. Journal of Colloid and Interface Science 41, 311-317.

Perry, A. P., Neipert, C., Space, B., Moor, P. B., 2006. Theoretical modelling of interface specific vibrational spectroscopy: methods and applications to aqueous interfaces. Chemical Reviews 106, 1234-1258.
Peterson, E. S., Harris, C. B., 1989. A new technique for the determination of surface adsorbate geometries utilizing second harmonic generation and absorption band shifts. Journal of Chemical Physics 91, 2683-2688.
Sato, M., Kaieda, T., Ohmukai, K., Kawazumi, H., Harata, A., Ogawa, T., 2000. Acid-base equilibrium constants at the water surface and distribution coefficients between the surface and the bulk as studied by the laser two-photon ionization technique. Journal of Physical Chemistry 104, 9873-9877.
Sato, M., Akagishi, H., Harata, A., Ogawa, T., 2001. Polarization and surface density dependence of pyrenehexadecanoic acid at the air-water interface under compression studied by a laser two-photon ionization. Langmuir, 17, 8167-8171.
Sato, M., Harata, A., Hatano, Y., Ogawa, T., Kaieda, T., Ohmukai, K., Kawazumi, H., 2004. Acid-base equilibrium constants and distribution coefficients of aminopyrene between the surface and bulk of liquid water as studied by a laser two-photon ionization technique. Journal of Physical Chemistry 108, 12111-12115.
Seno, K., Ishioka, T., Harata, A., Hatano, Y., 2001. Multi-Photon Ionization of Rhodamine Dyes Adsorbed at the Aqueous Solution Surfaces. Abstracts for ASIANALYSIS VI (Yoyogi, Japan, 2001), 28.
Seno, K., Ishioka, T., Harata, A., Hatano, Y., 2002. Photoionization of rhodamine dyes adsorbed at the aqueous solution surfaces investigated by synchrotron radiation. Analytical Sciences 17 special issue, i1177-1179.
Shen, Y. R., 1989. Optical second harmonic generation at interfaces. Annual Review of Physical Chemistry 40, 327-350.
Shen, Y. R., Ostroverkhov, V., 2006. Sum-frequency vibrational spectroscopy on water interfaces: polar orientation of water molecules at interfaces. Chemical Reviews 106, 1140-1154.
Slyadneva, O. N., Slyadnev, M. N., Tsukanova, V. M., Inoue, T., Harata, A., Ogawa, T., 1999. Orientation and aggregation behavior of rhodamine dye in insoluble film at the air–water interface under compression: second harmonic generation and spectroscopic studies. Langmuir 15, 8651-8658.
Slyadneva, O. N., Slyadnev, M. N., Harata, A., Ogawa, T., 2001. Second harmonic generation from the mixed films of rhodamine dye and arachidic acid at the air-water interface: correlation with spectroscopic properties, role of spacer molecules in the monolayer. Langmuir 17, 5329-5336.
Slyadneva, O. N., Harata, A., Hatano, Y., 2003. Second harmonic generation from insoluble films of a rhodamine dye at the air/water interface: effect of sodium dodecylsulfate. Journal of Colloid and Interface Sciences 260, 142-148.
Tashiro, K., Ishioka, T., Harata, A., 2003. Analysis of the oil/water interface probed by laser-multiphoton ionization of rhodamine dyes. Proceedings of the 5th Cross Straits Symposium on Materials, Energy and Environmental Sciences (Pusan, Korea, 2003), pp 61-62.
Timoshenko, M. M., Korkoshko, I. V., Kleimenov, V. I., Petrachenko, N. E., Chizhov, Y. V., Ryl'kov, V. V., Akopyan, M. E., 1981. Ionization potentials of rhodamine dyes. Doklady Akademii Nauk SSSR 260, 138-140.

Tsukanova, V., Harata, A., Ogawa, T., 2000. Second-harmonic probe of pressure-induced structure ordering within long-chain fluorescence monolayer at the air/water interface. Journal of Physical Chemistry B 104, 7707-7712.
Voigtman, E., Jurgensen, A., Winefordner, J. D., 1981. Comparison of laser excited fluorescence and photoacoustic limits of detection for static and flow cells. Analytical Chemistry 53, 1921-23.
Voigtman, E., Winefordner, J. D., 1982. Two-photon photoionization detection of polycyclic aromatic hydrocarbons and drugs in a windowless flow cell. Analytical Chemistry 54, 1834-1989.
Watanabe, I., Flanagan, J. B., Delahay, P., 1980. Journal of Chemical Physics 73, 2057-2062.
Watanabe, I., Ikeda, S., 1983. Study of solutions by photoemission spectroscopy. Kagaku (Kyoto, Japan) 38, 14-20 (in Japanese).
Watanabe, I., 1994. Optical oxidation potential: a new measure for reducing power. Analytical Sciences 10, 229-239.
Watanabe, I., Takahashi, N., Tanida, H., 1998. Dehydration of iodide segregated by tetraalkylammonium at the air/solution interface studied by photoelectron emission spectroscopy. Chemical Physics Letters 287, 714-718.
Watanabe, I., 2006. Analytical methods for surfaces, interfaces and boundary regions - photoelectron as a probe for the solution surface study. Bunseki 3, 102-108 (in Japanese).
Winter, B., Faubel, M., 2006. Photoemission from liquid aqueous solutions. Chemical Reviews 106, 1176-1211.
Yamada, S., Kano, K., Ogawa, T., 1982. Laser two-photon ionization technique for a highly sensitive detection of pyrene. Bunseki Kagaku 31, E247-E250.
Yamada, S., Hino, A., Kano, K., Ogawa, T., 1983. Laser two-photon ionization for determination of aromatic molecules in solution. Analytical Chemistry 55, 1914-1917.
Yamada, S., Ogawa, T., Zhang, P., 1986. Trace determination of some aromatic molecules by laser two-photon ionization. Analytica Chimica Acta 183, 251-256.
Zhao, X., Subrahmanyan, S., Eisenthal, K. B., 1990. Determination of pK_a at the air/water interface by second harmonic generation. Chemical Physics Letters 171, 558-562.
Zheng, X.-Y., Harata, A., Ogawa, T., 2000. Fluorescence photon bursts from low surface-density dioctadecyl-rhodamine B molecules at the air-water surface observed with a confocal fluorescence photon-counting microscope. Chemical Physics Letters 316, 6-12.
Zheng, X.-Y., Harata, A., 2001a. Confocal fluorescence microscope studies of the adsorptive behavior of dioctadecyl-rhodamine B molecules at a cyclohexane-water interface. Analytical Sciences 17, 131-135.
Zheng, X.-Y., Harata, A., Ogawa, T., 2001b. Study of the adsorptive behavior of water-soluble dye molecules (rhodamine 6G) at the air-water interface using confocal fluorescence microscope. Specrtochimca Acta Part A 57, 315-322.
Zheng, X.-Y., Wachi, M., Harata, A., Hatano, Y., 2004. Acidity effects on the adsorptive behavior and fluorescence properties of rhodamine 6G molecules at

the air-water interface studied with confocal fluorescence microscopy. Specrtochimca Acta Part A 60, 1085-1090.

Table 1

Photoionization thresholds (eV) of chemicals on the water surface determined with the exponent of 2.5. The pH value of the water subphase is adjusted. The major chemical form is indicated in parentheses. The molecular density is controlled: coverage, <0.74 %. 1-aminopyrene and 1-pyrenebutyric acid are slightly soluble in water, 1-pyrenehexadecanoic acid is insoluble, and rhodamine 6G is soluble.

1-aminopyrene		**rhodamine 6G**	
pH 1.05 (cation)	5.7_2	pH 1 (cation)	5.7_9
pH 7.02 (neutral)	5.4_5	pH 3 (cation)	5.7_4
1-pyrenebutyric acid		pH 7 (cation)	5.6_7
pH 3.11 (neutral)	6.0_9	**rhodamine B**	
pH 11.19 (anion)	5.8_8	pH 7 (zwitterion)	5.6
1-pyrenehexadecanoic acid		**rhodamine 101**	
pH 3.11 (neutral)	6.0_7	pH 7 (zwitterion)	5.3
pH 11.19 (anion)	5.8_7		

Refs.: Ionization potential (eV)

aminopyrene	6.8 ± 0.1	(CTS, Farrell and Newton, 1966)
pyrene	7.426	(NIST Chemistry WebBook, Online, 2002)
rhodamine B	6.7	(Timoshenko et al., 1981)

Table 2

Adsorption equilibrium coefficients K_{ad} and signal intensity factors (Q_{max} and S_{max}) evaluated from each experiment. Q_{max}, signal intensity factors of two-photon ionization measurements with one unit of fC. The polarization is of the excitation laser. S_{max}, signal intensity factors of second harmonic generation measurements with an arbitrary unit.

dye	Polarization	Q_{max} (fQ), S_{max} (arb. units)	K_{ad} (10^5 M^{-1})
Two photon ionization measurements			
rhodamine B	s	87	6.1
	p	72	7.4
rhodamine 6G	s	4.5	21
	p	6.0	27
Second harmonic generation measurements			
rhodamine B	s	2.3	4.1
	p	3.9	4.0
rhodamine 6G	s	9.3	1.2
	p	7.7	2.2

Table 3

Some properties of rhodamine dyes for adsorption at the water surface at room temperature (25 °C) determined with surface tension measurements by assuming the Langmuir adsorption isotherm. K_{ad}, equilibrium constant; N_{max}, molecular density at the adsorption saturation; and A_{min}, specific molecular area at the adsorption saturation.

dye	K_{ad} (10^5 M^{-1})	N_{max} (10^{-7} mol/m^2)	A_{min} (nm^2/molecule)
rhodamine B	8.8	6.7	2.5
rhodamine 6G	58	1.0	16.5
rhodamine 110	6.3	4.3	3.8

Table 4

Detection limit (3σ) of some water-soluble molecules at the water surface, shown in bulk concentration. Excess energy is calculated as $E_{excess} = (E_{S_1} + h\nu) - E_{th}$, where E_{S_1} is the energy of the first excited singlet state determined from absorption spectra, $h\nu$ is the photon energy, and E_{th} is the energy of the photoionization threshold determined from the photoionization spectra. The partition coefficients P(o/w) between *n*-octanol and water were estimated with Chem3D Ultra6.0 (Cambridge Soft Corp.).

compound	*excitation wavelength* (nm)	*molar absorptivity* ($M^{-1}cm^{-1}$)	E_{excess} (eV)	log*P*(o/w)	detection limit (nM)
rhodamine B	337	2000	0.20	2.13	41
pyrene	337	15000	0.90	5.18	0.044
1-aminopyrene	337	13200	0.62	3.72	0.094
anthracene	337	5900	1.85	4.49	0.39
	355	5100	1.07		0.40
1-chloroanthracene	355	3600	0.62	5.20	0.22
9,10-dichloroanthracene	355	5000	0.90	5.92	0.20

* The values of the detection limits, molar absorptivity, and excess energy for the excitation wavelength of 337 nm and 355 nm are referred from Inoue et. al. (1994) and Chen et al. (1994) , respectively.

Figure Captions

Fig. 1.
Time-average mass density distribution at the pure water surface at 300K.

Fig. 2.
Relationship between concentration and surface density for rhodamine dyes. The concentration ranges for an observation with a variety of methods are shown. The surface density ranges should be calculated from the concentration range with the relationship between the concentration and surface density (solid curves).

Fig. 3.
Interactions of a laser light with molecules at an interface.

Fig. 4.
Schematic illustration for the detection of the photoionization current from molecules adsorbed at the water surface.

Fig. 5.
Experimental setup for measuring the photoionization current spectra of molecules adsorbed at the water surface.

Fig. 6.
Left: Typical time profile of a measured laser two-photon ionization current of an aqueous solution of rhodamine B chloride (10 μM). The laser pulse energy was 0.25 mJ/pulse. The peak current was 22 nA, and the ionization charge determined as time-integrated current was 160 fC. (Inset) Schematic illustration of the experimental setup around the sample. Right: Pump pulse-energy dependence of the ionization current amplitude for an aqueous solution of rhodamine B chloride. The excitation wavelength was 355 nm.

Fig. 7.
Photocurrent spectra of 1-aminopyrene at the aqueous solution surfaces with different pH values. The photocurrents are normalized with the ring current but not with light intensity measured. High-energy photons are cut with a quartz plate.

Fig. 8.
Photocurrent spectra of rhodamine 6G chloride (R6G) at the aqueous solution surfaces with different pH values. The photocurrents are normalized with the ring current but not with light intensity. The decrease in the light intensity around 6.8-8.4 eV is due to light absorption by water vapor. The signal around

5.0-5.4 eV is due to the insufficient cut of second-order light at 10.0-10.8 eV because a quartz plate was not inserted in the light path.
The chemical structures and direction of the molecular axis are shown for rhodamine 6G as well as rhodamine B chloride (RhB) and rhodamine 101 perchlorate (Rh101) for later discussion.

Fig. 9.
Fitting of a photocurrent spectrum of 1-aminopyrene to the empirical equation: (a), photocurrent spectrum and fitting results with single (n=2.5, 3.5) and double (n=2.5) components; (b), dependence of the estimated photoionization threshold energy on exponent n; (c), dependence of the summation of the squared residual errors on exponent n in the single component analysis; and (d), dependence of the summation of the squared logarithmic residual errors on exponent n in the single-component analysis.

Fig. 10.
Effect of arachidic acid addition on the photocurrent from the surface of rhodamine B aqueous solution measured by single-photon ionization (left) and measured by two-photon ionization (right). Error bars indicate deviations of current intensities for each laser pulse.

Fig. 11.
Left: Concentration dependence of the ionization charge of an aqueous solution of rhodamine dyes when s- or p-polarized laser light excited the surfaces of aqueous solutions of rhodamine B chloride (RhB) and rhodamine 6G chloride (R6G). The curves are the fitting results of the experimental data to the Langmuir isotherm. Right: Concentration dependence of the second harmonic generation signal intensity from the surface of aqueous solutions of rhodamine dyes when s- or p-polarized laser light at 532 nm excited the surfaces of aqueous solutions of RhB and R6G. The curves are the fitting results of the experimental data to the Langmuir isotherm. Polarization is that of the excitation laser. The polarization of the second harmonic light at 266 nm is not selected.

Fig.12.
Left: Concentration dependence of the surface tension for aqueous solutions of rhodamine B chloride (RhB), rhodamine 6G chloride (R6G), and rhodamine 101 perchlorate (Rh101) at 25 C°. Right: Ultraviolet-visible absorption spectra of aqueous solutions of rhodamine dyes.

Fig. 13.
Right: Dependence of the photoionization signal intensity $I(\theta)$ on the polarization angle θ of the excitation laser at 355 nm and 84 degrees of incident angle for 4 sets of concentrations of an aqueous solution of rhodamine dyes:

rhodamine B chloride (RhB) and rhodamine 6G chloride (R6G). θ=0 deg and θ =90 deg for p- and s-polarized light, respectively, and $I_s = I(\theta$=90 deg). The curves are the fitting results of the experimental data to sinusoidal functions. The arrows indicate the order of the sample concentrations listed at the right-hand side of them. Left: Concentration dependence of the photoionization ratio I_p/I_s and surface excess for an aqueous solution of rhodamine dyes: RhB and R6G). The surface excess is calculated with the adsorption properties listed in Table 3.

Fig. 14.
Right: Dependence of the photoionization charge on the surface excess of rhodamine B on the water. Left: Dependence of the photoionization charge on the surface excess of rhodamine 6G on the water. The surface excess is calculated with the adsorption properties listed in Table 2.

Fig. 15.
Rough sketch of rhodamine dyes at the water surface. The arrows indicate the direction of molecular motion in increasing concentration in bulk solution. The short axis of the rhodamine B (RhB) molecule is relatively parallel to the water surface, while the long and short axes of the rhodamine 6G (R6G) molecule have large angles with respect to the water surface. With a concentration increase, RhB changes the direction of the short axis, and R6G changes the directions of the long and short axes as well as the depth position.

Fig. 16.
pH-dependence of the 2-photon ionization signal for (left) 1-aminopyrene and (right) 1-pyrenebutyric acid on the water surface. The subphase pH and ionic strength are adjusted with NaH_2PO_4 and HCl and 1.0M KCl.

Fig. 17.
Photoionization spectra of p-xylene at the water surface after 10 μL p-xylene is spread on the 9.08 cm^2 area of the water surface. The photocurrents are normalized with the ring current but not with light intensity. The spectra shape reflects the photoabsorption of water vapor in the gas phase above the water as well as the spectrum of the light source and the photoionization threshold of p-xylene.

Fig. 18.
Photoionization current at the water surface after 3 μL benzene is spread on the 9.08 cm^2 area of the water surface. The photocurrents are normalized with the ring current but not with light intensity.

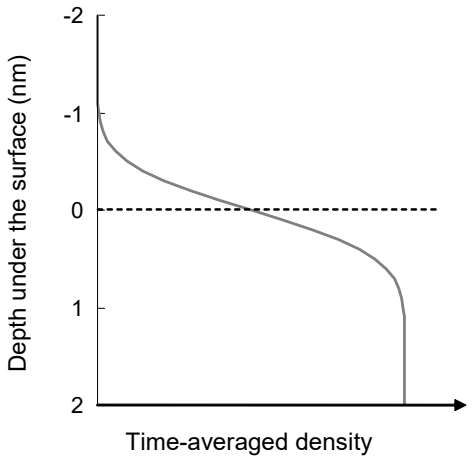

Fig. 1 Harata et al.

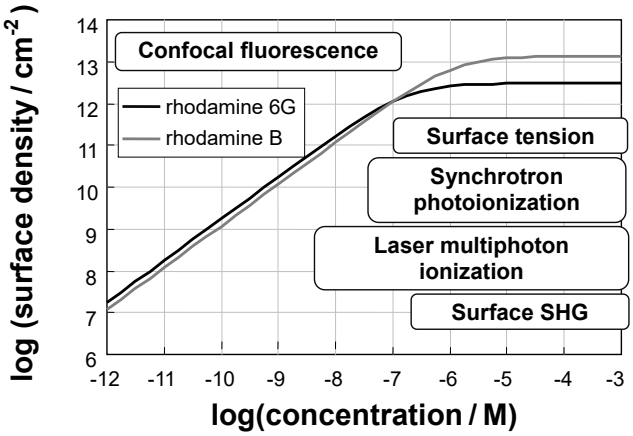

Fig. 2 Harata et al.

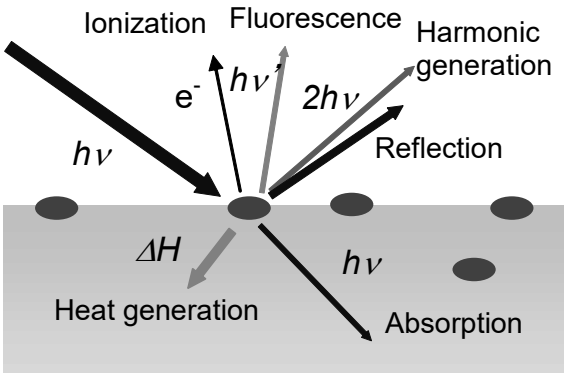

Fig. 3 Harata et al.

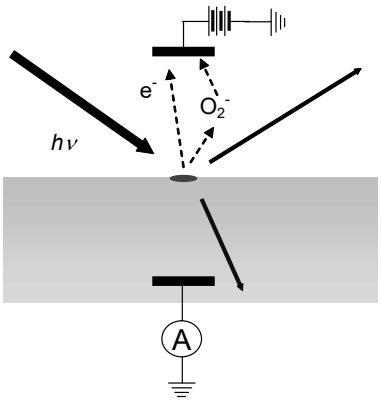

1

Fig. 4 Harata et al.

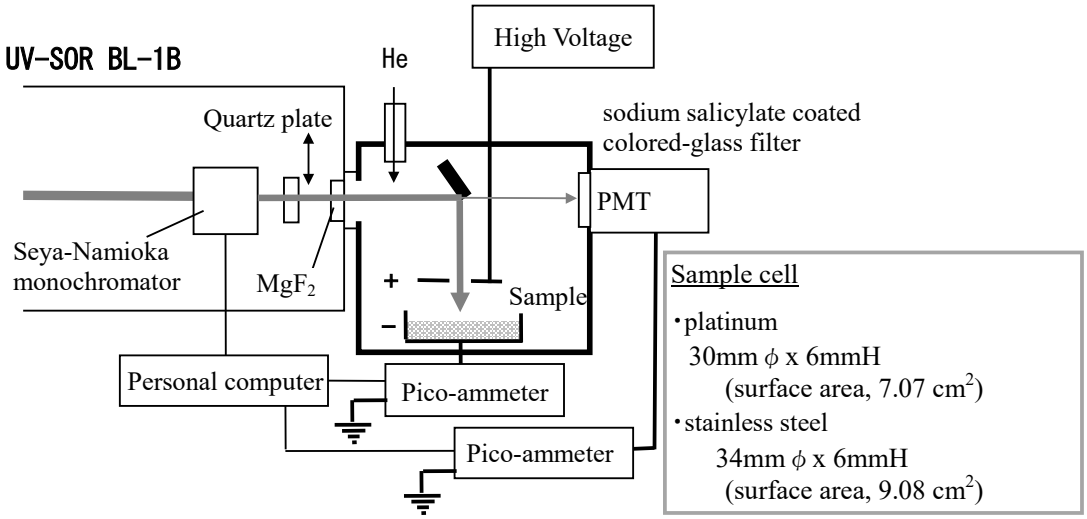

Fig. 5 Harata et al.

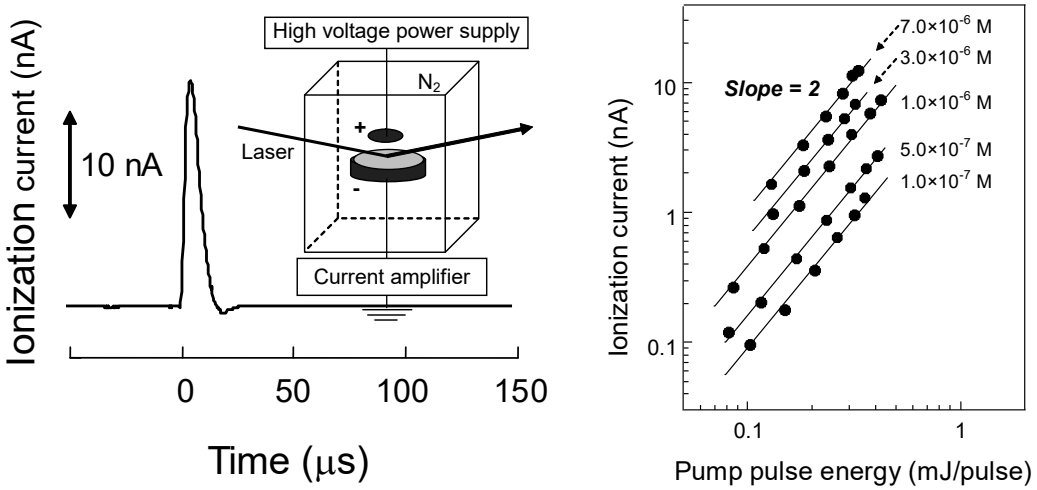

Fig. 6 Harata et al.

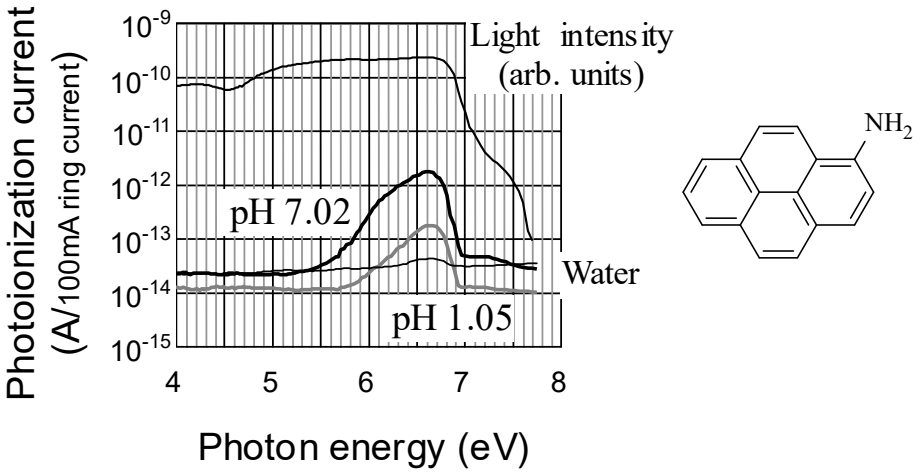

Fig. 7 Harata et al.

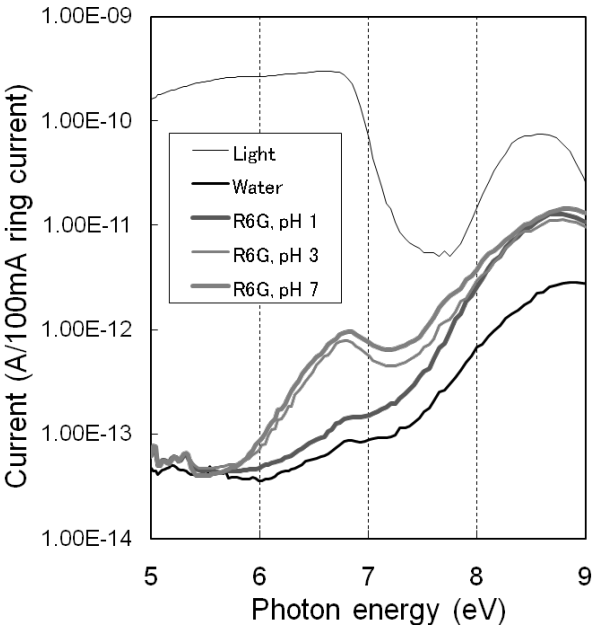

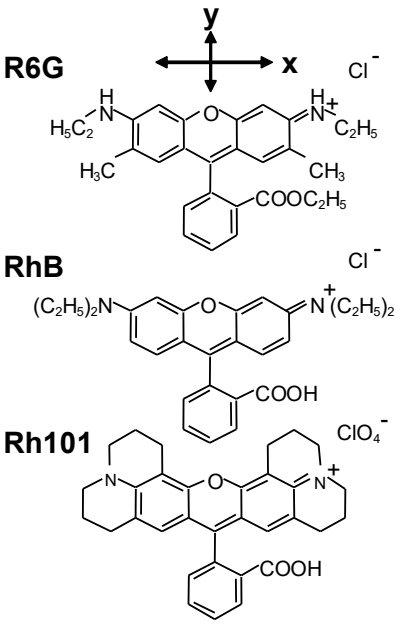

Fig. 8 Harata et al.

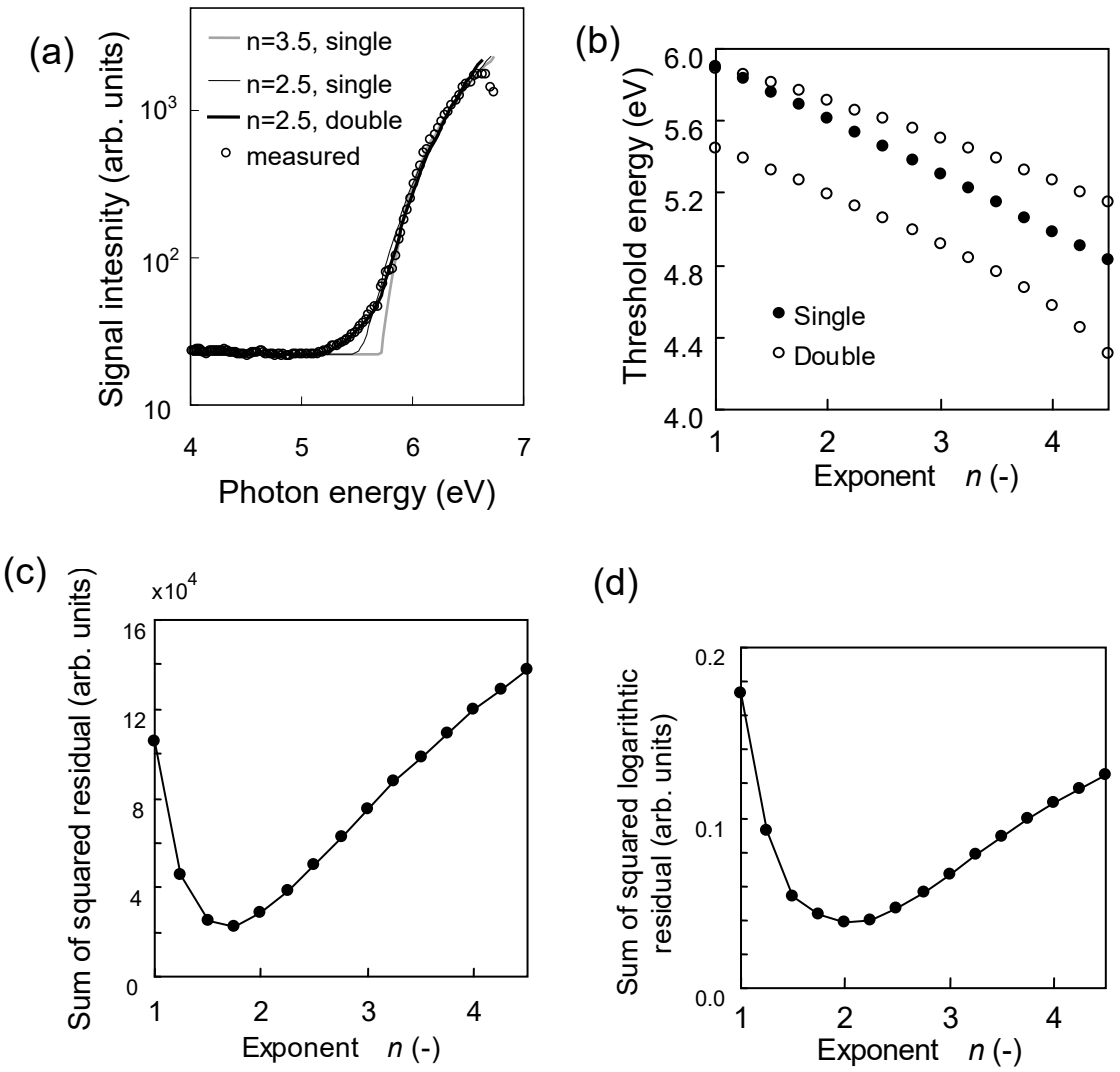

Fig. 9 Harata et al.

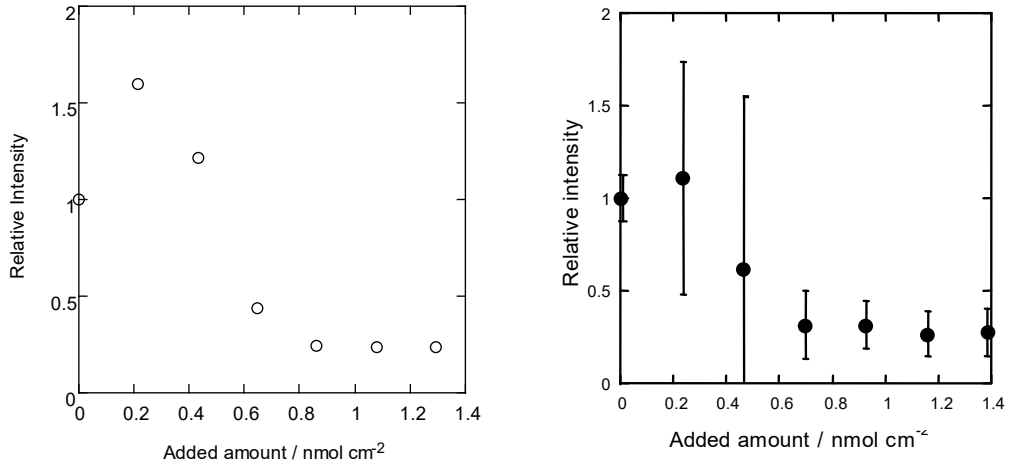

Fig. 10 Harata et al.

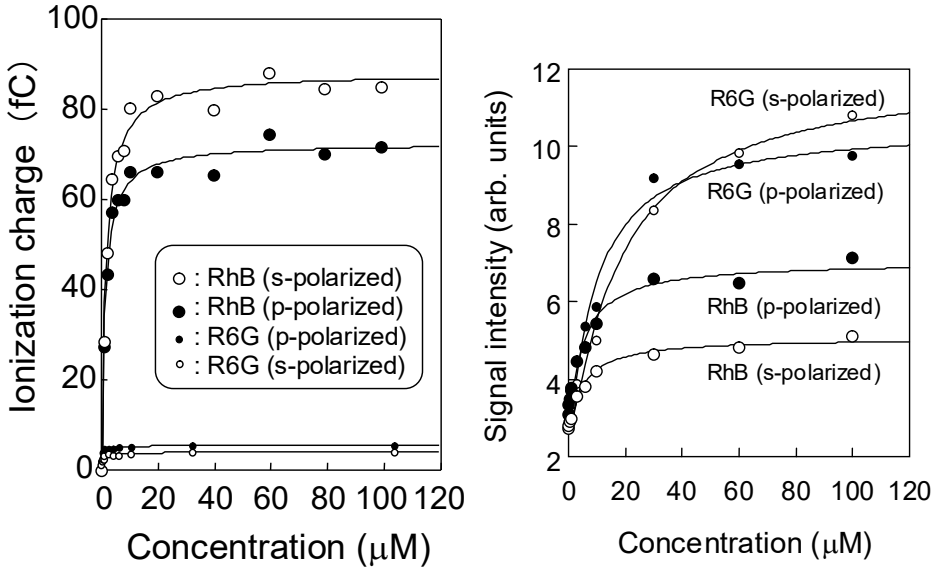

Fig. 11 Harata et al.

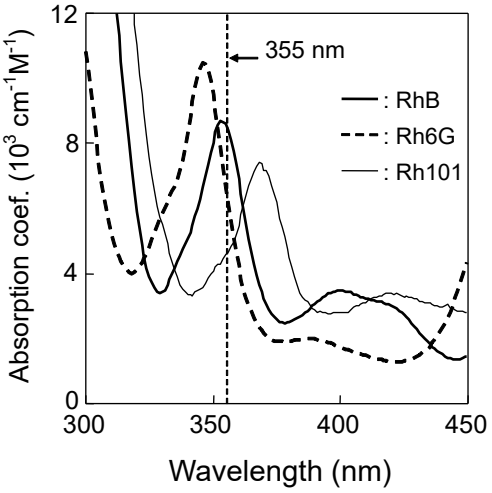

Fig. 12 Harata et al.

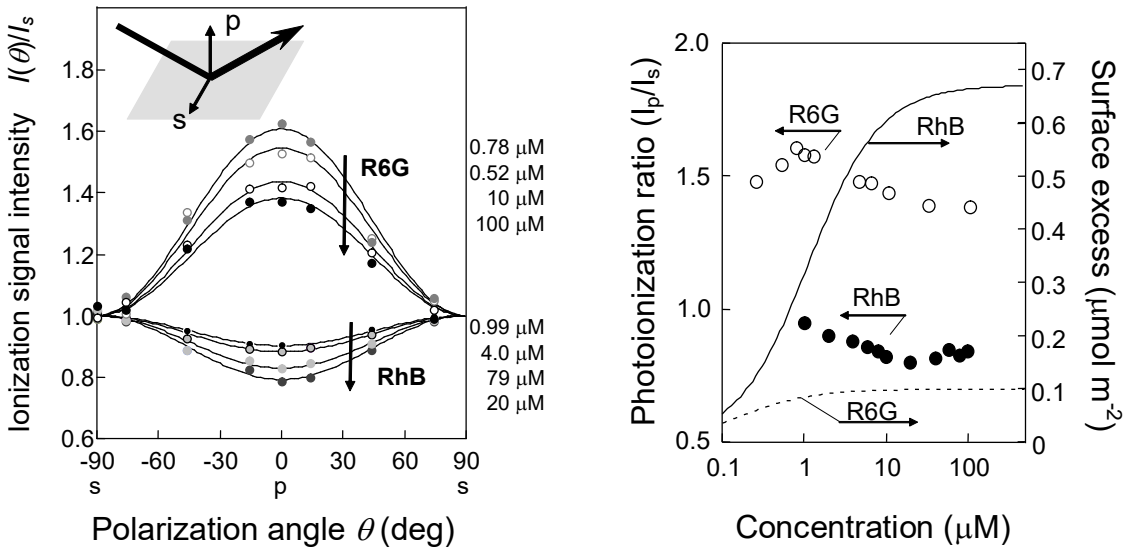

Fig. 13 Harata et al.

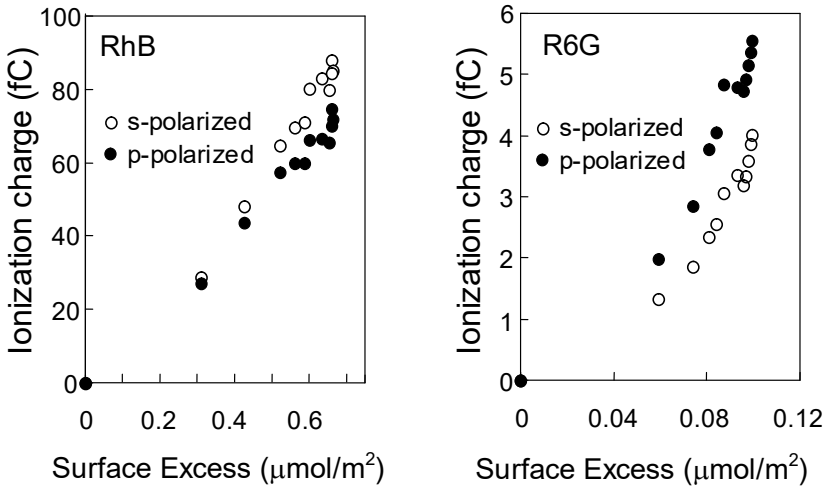

Fig. 14 Harata et al.

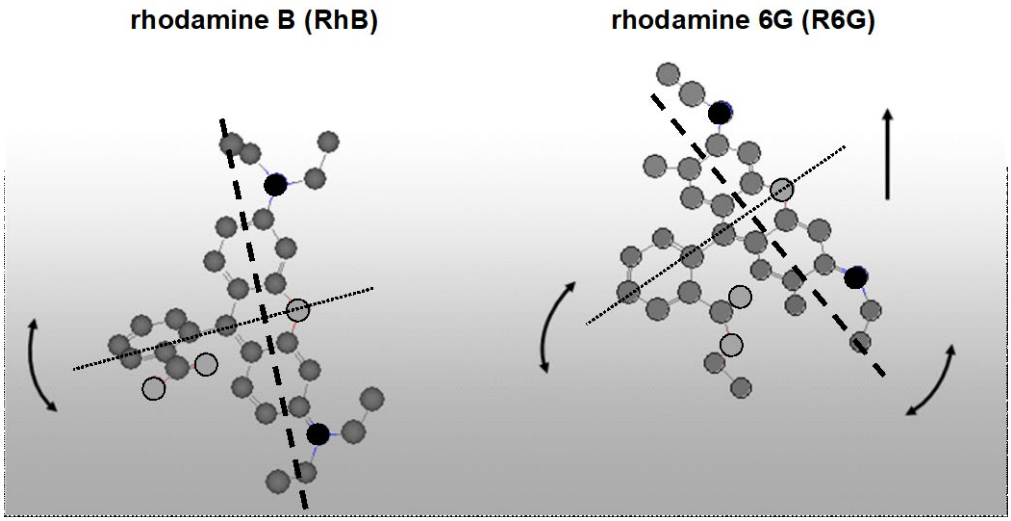

Fig. 15 Harata et al.

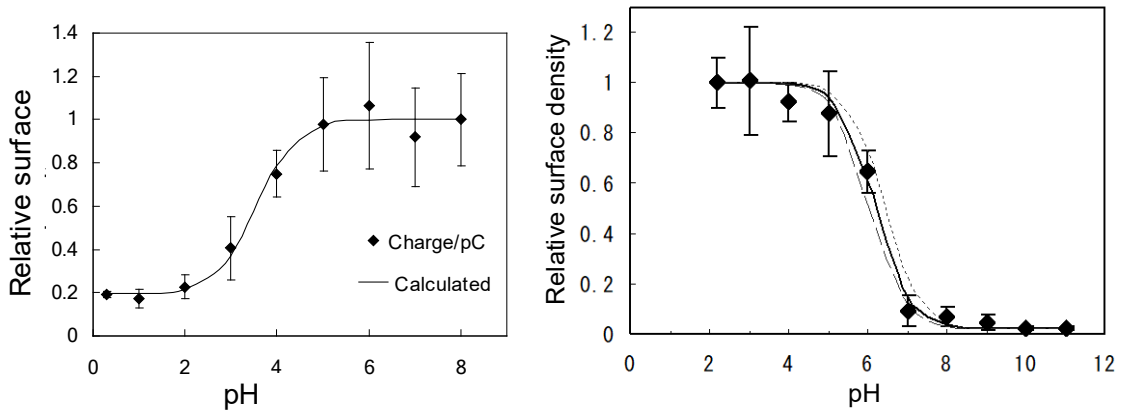

Fig. 16 Harata et al.

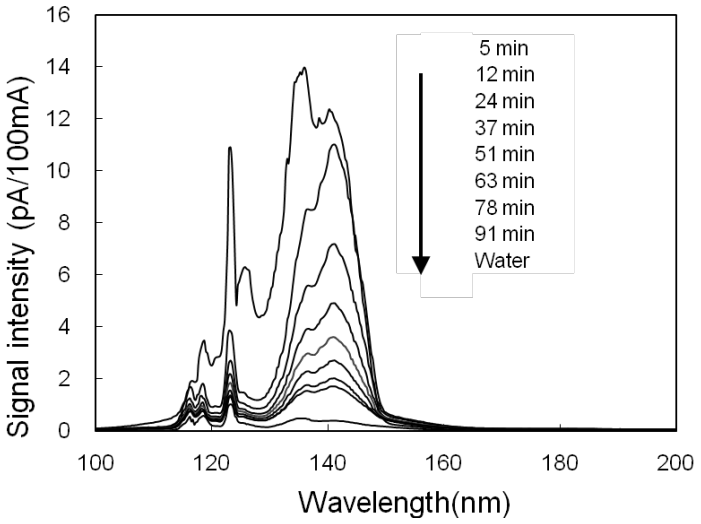

Fig. 17 Harata et al.

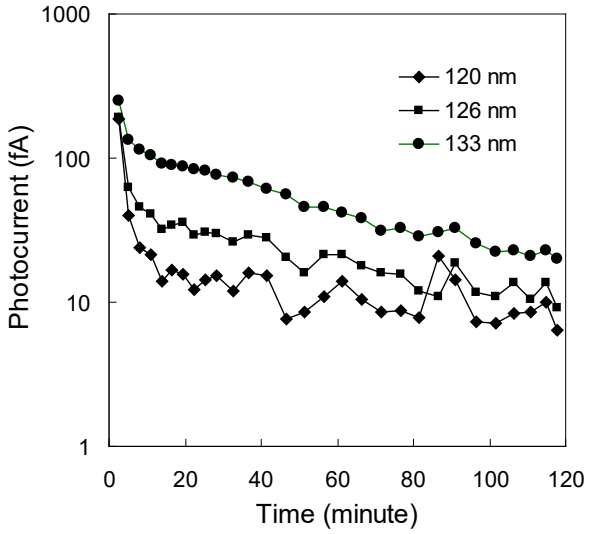

Fig. 18 Harata et al.